MITSUBISHI ELECTRIC RESEARCH LABORATORIES
http://www.merl.com

Online Blind Deconvolution for Sequential Through-the-Wall-Radar-Imaging

Mansour, H.; Kamilov, U.; Liu, D.; Orlik, P.V.; Boufounos, P.T.; Parsons, K.; Vetro, A.

TR2016-093 September 2016

Abstract

We propose an online blind deconvolution approach to sequential through-the-wall-radar-imaging (TWI) where the received signal is contaminated by front wall ringing artifacts. The sequential measurements correspond to individual transmitter-receiver pairs where the front wall ringing induces a multipath kernel that corrupts the received target reflections. The convolution kernels may vary across sequential measurements but are assumed to be shared among targets viewed by a single measurement. Our approach extends recent convex programming formulations for blind deconvolution to the sequential measurement scenario by formulating it as a low-rank tensor recovery problem. We develop a stochastic gradient descent algorithm that is capable of recovering the sparse scene and separating out the delay convolution kernels. We demonstrate the recovery capabilities of our approach on a synthetic scene as well as with real TWI radar measurements.

2016 International Workshop on Compressed Sensing Theory and its Applications to Radar, Sonar, and Remote Sensing (CoSeRa)

Online Blind Deconvolution for Sequential Through-the-Wall-Radar-Imaging

Hassan Mansour, Ulugbek Kamilov, Dehong Liu, Philip Orlik,
Petros Boufounos, Kieran Parsons, Anthony Vetro
Mitsubishi Electric Research Laboratories
Cambridge, MA 02139, USA
Email: {mansour, kamilov, liudh, porlik, petrosb, parsons, avetro}@merl.com

***Abstract*—We propose an online blind deconvolution approach to sequential through-the-wall-radar-imaging (TWI) where the received signal is contaminated by front wall ringing artifacts. The sequential measurements correspond to individual transmitter-receiver pairs where the front wall ringing induces a multipath kernel that corrupts the received target reflections. The convolution kernels may vary across sequential measurements but are assumed to be shared among targets viewed by a single measurement. Our approach extends recent convex programming formulations for blind deconvolution to the sequential measurement scenario by formulating it as a low-rank tensor recovery problem. We develop a stochastic gradient descent algorithm that is capable of recovering the sparse scene and separating out the delay convolution kernels. We demonstrate the recovery capabilities of our approach on a synthetic scene as well as with real TWI radar measurements.**

I. Introduction

In Through-the-wall-imaging (TWI), the received radar signal reflected from the targets is often corrupted with indirect multipath reflections from front wall ringing as well as reflections off internal structures. This phenomenon often results in ghost artifacts that clutter the reconstructed radar image. Suppressing such multipath reflections can significantly improve the quality of TWI and enhance the applicability of the technique.

Several works have considered the problem of multipath elimination by assuming perfect knowledge of the reflective geometry of the scene [1]–[4]. These works either model the propagation physics or build sparsifying dictionaries that incorporate the sources of the multipath reflections in order to remove artifacts. Other approaches formulate TWI as a blind sparse-recovery problem where the wall parameters and the sources of multipath are not known [5], [6]. While [5] modeled the multipath effect as a delay kernel convolved with a sparse primary impulse response of the targets in the scene, [6] adopted a sparsity-based multipath exploitation framework by allowing for uncertainties in wall-parameters that are solved via an alternating optimization scheme.

We are interested in a TWI signal model where the target reflections are convolved with an unknown delay-multipath kernel due to the front wall ringing. In particular, we address a scenario where the receivers obtain their measurements sequentially, and where multipath reflections of all targets are generated by a convolution kernel that may change between different receivers. This setup is particularly suitable when the antennas are directional and the targets are offset from the antennas by a large standoff distance. This scenario was addressed in [7] by proposing an online blind deconvolution heuristic, based on sparse Kaczmarz iterations, to separate the target reflections from the multipath kernels.

Recently, [8], [9] proposed convex programming solutions for blind deconvolution. Consider a signal $\mathbf{r} \in \mathbb{R}^{N_t}$ composed of the convolution of a kernel $\mathbf{d} = \mathbf{B}\mathbf{h}, \mathbf{h} \in \mathbb{C}^{N_h}$ and a signal $\mathbf{y} = \mathbf{A}\mathbf{x}$ restricted to the span of the columns of a matrix $\mathbf{A} \in \mathbb{C}^{N_t \times M}$. Denote by $\mathbf{X}_o = \mathbf{h}\mathbf{x}^H$ the lifted space signal composed of the outer product of $\mathbf{h}$ and $\mathbf{x}$. It was shown in [8] that the signals $\mathbf{h}$ and $\mathbf{x}$ can be resolved from $\mathbf{r}$ by solving a convex nuclear norm minimization problem in the lifted space when N_h and $M < cN_t$, $0 < c < 1$ and for certain conditions on $\mathbf{A}$ and $\mathbf{B}$. Ling and Strohmer [9] later generalized the model to the case where $M > N_t$ but $\mathbf{x}$ is K-sparse with $KN_h < c'N_t$, $0 < c' < 1$, by solving an ℓ_1 minimization problem in the lifted space.

In this paper, we extend the developments in [8], [9] to the sequential TWI measurement model described in Section II. Let $\mathbf{r}_j = \mathbf{d}_j * \mathbf{y}_j$ be a single measurement observed by a transmitter-receiver pair indexed by $j \in \{1 \dots J\}$. The measurement $\mathbf{r}_j$ is composed of the convolution of a multipath kernel $\mathbf{d}_j = \mathbf{B}\mathbf{h}_j$ and the target impulse response $\mathbf{y}_j = \mathbf{A}_j\mathbf{x}$. Our objective is to recover the sparse target reflectivity vector $\mathbf{x}$ that is common across all the J measurements. We propose a low rank tensor recovery problem in Section III in which the tensor is composed of stacking the rank-1 outer product matrices $\mathbf{X}_j = \mathbf{h}_j\mathbf{x}^H$. To that end, we propose a stochastic gradient descent algorithm that acts on the individual measurements $\mathbf{r}_j$ to separate the signals $\mathbf{d}_j$ from $\mathbf{y}_j$ and consequently recover the sparse target reflectivity $\mathbf{x}$. We evaluate the performance of our scheme in Section IV by applying it to a synthetic scene as well to real TWI radar measurements.

II. Front Wall Ringing Model

We consider a radar setup with N_s transmitting sources and N_r receiving antennas. Let $s(t)$ be the time-domain waveform of the pulse that is transmitted by each source. Denote by $g_p(t, n_r, n_s)$ the primary impulse response of the scene, excluding multi-path reflections, viewed at receiver $n_r \in \{1, \dots N_r\}$ as a reflection of a pulse transmitted from source $n_s \in \{1, \dots N_s\}$. Also denote by $g_m(t, n_r, n_s)$ the impulse response of the multi-path reflections due to the front wall ringing. Using a standard time-domain representation of the received signal model, we express the received signal

$r(t, n_r, n_s)$ as follows

$$r(t, n_r, n_s) = s(t) * (g_p(t, n_r, n_s) + g_m(t, n_r, n_s)), \quad (1)$$

where $*$ is the convolution operator.

Without loss of generality, suppose that there are K targets in the scene, each inducing a primary impulse response $g_k(t, n_r, n_s)$ indexed by $k \in \{1 \dots K\}$. The multiples' impulse response can then be modeled by the convolution of a delay kernel $d(t, n_r, n_s)$ with the primary impulse response $g_k(t, n_r, n_s)$ of each target object in the scene, such that,

$$\begin{aligned} g_p(t, n_r, n_s) &= \sum_{k=1}^{K} g_k(t, n_r, n_s), \\ g_m(t, n_r, n_s) &= d(t, n_r, n_s) * \left(\sum_{k=1}^{K} g_k(t, n_r, n_s) \right). \end{aligned} \quad (2)$$

In what follows, we use $d(t, n_r, n_s)$ as an activation function that generates both the primary and multiple impulse responses. Consequently, the received signal model can be written as the superposition of the primary responses of all K objects in the scene convolved with an activation function as follows

$$r(t, n_r, n_s) = s(t) * \sum_{k=1}^{K} d(t, n_r, n_s) * g_k(t, n_r, n_s), \quad (3)$$

where $d(t, n_r, n_s)$ is independent of k.

III. Multipath Removal as Online Blind Deconvolution

A. Problem formulation

Let j be an index of the transmitter-receiver pair $(n_r, n_s) \in [N_r] \times [N_s]$ and let $M = N_x N_y N_z$. Denote by $\mathbf{r}_j \in \mathbb{R}^{N_t}$ the received signal at transmitter and receiver locations (n_r, n_s), where N_t is the number of time samples recorded by a receiver for each transmission. Also denote by $\mathbf{d}_j \in \mathbb{R}^{N_t}$ the corresponding vectorized time-domain activation function. Let $\mathbf{S} : \mathbb{R}^{N_t} \to \mathbb{C}^{N_f}$ be the source waveform matched-filtering operator that maps $\mathbf{r}_j$ to its frequency domain matched-filtered response $\hat{\mathbf{r}}_j = \mathbf{S}\mathbf{r}_j$, where N_f is the number of sampled frequency bins. We discretize the scene into an $N_x \times N_y \times N_z$ grid and construct the imaging operator $\mathbf{G}_j : \mathbb{C}^{N_f} \to \mathbb{C}^M$ that maps $\hat{\mathbf{r}}_j$ to the image $\mathbf{x}$, such that

$$\mathbf{G}_j(\omega, l) = e^{\mathrm{i}\omega(\|\phi(l) - \phi(n_r)\|_2 + \|\phi(l) - \phi(n_s)\|_2)/c}, \quad (4)$$

where ω is the frequency in radians, l is a spatial index in $N_x \times N_y \times N_z$, c is the speed of the wave in free space, and $\phi(\cdot) \in \mathbb{R}^3$ gives the spatial coordinate vector of scene index l, receiver n_r, and transmitter n_s. Denote by $\mathbf{A}_j$ the $N_t \times M$ matrix $\mathbf{A}_j := \mathbf{S}^H \mathbf{G}_j^H$. The received signal model in (3) can now be expressed as a function of the image $\mathbf{x}$ as

$$\mathbf{r}_j = \mathbf{d}_j * \mathbf{A}_j \mathbf{x} + \mathbf{n}_j, \quad (5)$$

where $\mathbf{n}_j$ is a noise vector. The combined imaging and multipath removal problem can now be formulated as the following nonlinear inverse problem

$$\min_{\mathbf{x}, \mathbf{d}_j \forall j} \frac{1}{2} \sum_j \|\mathbf{r}_j - \mathbf{d}_j * \mathbf{A}_j \mathbf{x}\|_2^2. \quad (6)$$

As it stands, problem (6) is ill-posed. Fortunately, the signals $\mathbf{x}$ and $\mathbf{d}_j$ are structured in that $\mathbf{x}$ is sparse and $\mathbf{d}_j = \mathbf{B}\mathbf{h}_j$ with $\mathbf{B} = \begin{bmatrix} \mathbf{I}_{N_h} \\ \mathbf{0} \end{bmatrix}$ and $N_h < N_t$.

B. Convex blind deconvolution

1) Single measurement: The authors of [8] and [9] address the case of a single measurement $\mathbf{r} = \mathbf{d} * \mathbf{y}$, where $\mathbf{d} = \mathbf{B}\mathbf{h}$, $\mathbf{y} = \mathbf{A}\mathbf{x}$, and $\mathbf{B} \in \mathbb{C}^{N_t \times N_h}, \mathbf{A} \in \mathbb{C}^{N_t \times M}$. Denote by $\hat{\mathbf{b}}_n$ and $\hat{\mathbf{a}}_n$ the nth rows of the Fourier transforms of the matrices $\mathbf{B}$ and $\mathbf{A}$, respectively, and by $\hat{\mathbf{r}}$ the Fourier transform of the measurement vector $\mathbf{r}$.

When $M < cN_t$ for some $c \in (0, 1)$, [8] shows that for random matrices $\mathbf{A}$ and orthonormal matrices $\mathbf{B}$, the signals $\mathbf{h}$ and $\mathbf{x}$ can be recovered from $\mathbf{r}$ by showing that the minimizer of the following nuclear norm minimization problem

$$\min_{\mathbf{X}} \|\mathbf{X}\|_* \text{ subject to } \hat{\mathbf{r}}(n) = \mathrm{Tr}\left(\hat{\mathbf{a}}_n^H \hat{\mathbf{b}}_n \mathbf{X}\right), \ n = 1 \dots N_f \quad (7)$$

is the rank-1 matrix $\mathbf{X}_0 = \mathbf{h}\mathbf{x}^H$ with high probability. Here $\hat{\mathbf{r}}(n)$ is the nth entry of $\hat{\mathbf{r}}$. On the other hand, when $M > N_t$ and $\mathbf{x}$ is K-sparse, [9] shows that the minimizer of the following ℓ_1 norm minimization problem

$$\min_{\mathbf{X}} \|\mathbf{X}\|_1 \text{ subject to } \hat{\mathbf{r}}(n) = \mathrm{Tr}\left(\hat{\mathbf{a}}_n^H \hat{\mathbf{b}}_n \mathbf{X}\right), \ n = 1 \dots N_f \quad (8)$$

is the rank-1 matrix $\mathbf{X}_0 = \mathbf{h}\mathbf{x}^H$ with high probability if $N_h K < c' N_t$ for some $c' \in (0, 1)$.

2) Multiple measurements: In the case of multiple measurements, we cast the blind deconvolution problem as a sparse and low rank tensor recovery problem.

Let $\mathbf{X}_j = \mathbf{h}_j \mathbf{x}^H \in \mathbb{C}^{N_h \times K}$ and denote by $\mathbf{T} \in N_h \times K \times J$ the tensor composed of stacking the matrices $\mathbf{X}_j$. We follow a tensor matricization approach and propose the following tensor nuclear norm minimization problem

$$\min_{\mathbf{X}_j} \sum_j \|\mathbf{X}_j\|_* \text{ subject to } \hat{\mathbf{r}}_j(n) = \mathrm{Tr}\left(\hat{\mathbf{a}}_{jn}^H \hat{\mathbf{b}}_n \mathbf{X}_j\right), \ \forall j, n, \quad (9)$$

where $\hat{\mathbf{a}}_{jn}$ is the nth row of $\hat{\mathbf{A}}_j$, the Fourier transform of the matrix $\mathbf{A}_j$. Using the Frobenius norm proxy of the matrix nuclear norm [10]

$$\|\mathbf{X}\|_* = \inf_{\mathbf{x}, \mathbf{h}: \mathbf{X} = \mathbf{h}\mathbf{x}^H} \frac{1}{2} \left(\|\mathbf{x}\|_F^2 + \|\mathbf{h}\|_F^2 \right),$$

we recast the tensor recovery problem as follows

$$\begin{aligned} \min_{\mathbf{x}, \mathbf{h}_j} \quad & \tfrac{J}{2} \|\mathbf{x}\|_2^2 + \tfrac{1}{2} \sum_j \|\mathbf{h}_j\|_2^2 \\ \text{subject to} \quad & \hat{\mathbf{r}}_j(n) = (\hat{\mathbf{b}}_n \mathbf{h}_j)(\hat{\mathbf{a}}_{jn} \mathbf{x}), \ \forall j, n \end{aligned} \quad (10)$$

When $M > N_t$ and $\mathbf{x}$ is sparse, we may add a sparse regularizer and rewrite the constraint as follows

$$\begin{aligned} \min_{\mathbf{x}, \mathbf{h}_j} \quad & \tfrac{J}{2} \|\mathbf{x}\|_2^2 + \tfrac{1}{2} \sum_j \|\mathbf{h}_j\|_2^2 + \lambda \|\mathbf{x}\|_1 \\ \text{subject to} \quad & \hat{\mathbf{r}}_j = \mathbf{D}_{\hat{\mathbf{B}}\mathbf{h}_j} \hat{\mathbf{A}}_j \mathbf{x}, \ \forall j, \end{aligned} \quad (11)$$

where $\mathbf{D}_{\mathbf{u}}$ constructs a diagonal matrix with the vector $\mathbf{u}$ on the diagonal, and $\hat{\mathbf{B}}$ is the Fourier transform of $\mathbf{B}$. Note that the following identity holds $\hat{\mathbf{r}}_j = \mathbf{D}_{\hat{\mathbf{B}}\mathbf{h}_j} \hat{\mathbf{A}}_j \mathbf{x} = \mathbf{D}_{\hat{\mathbf{A}}_j \mathbf{x}} \hat{\mathbf{B}} \mathbf{h}_j$.

C. Alternating stochastic gradient descent for sequential TWI

We start by rewriting (11) in unconstrained form as the regularized least squares problem

$$\min_{\mathbf{x},\mathbf{h}_j} F(\mathbf{x},\mathbf{h}_j) + G(\mathbf{x},\mathbf{h}_j), \tag{12}$$

where $F(\mathbf{x},\mathbf{h}_j) = \sum_j f_j(\mathbf{x},\mathbf{h}_j)$ with $f_j(\mathbf{x},\mathbf{h}_j) = \frac{1}{2}\|\hat{\mathbf{r}}_j - \mathbf{D}_{\hat{\mathbf{B}}\mathbf{h}_j}\hat{\mathbf{A}}_j\mathbf{x}\|_2^2$, and $G(\mathbf{x},\mathbf{h}_j) = \sum_j g_j(\mathbf{x},\mathbf{h}_j) + \lambda\|\mathbf{x}\|_1$, with $g_j(\mathbf{x},\mathbf{h}_j) = \frac{1}{2}\left(\|\mathbf{x}\|_2^2 + \|\mathbf{h}_j\|_2^2\right)$.

Since the measurements are acquired sequentially, we construct the quadratic approximation functions of $\mathbf{x}$ and $\mathbf{h}_j$ as follows

$$\begin{aligned} q_{\mathbf{x}}(\mathbf{x},\mathbf{x}^l,\mathbf{h}^l) &= (\mathbf{x}-\mathbf{x}^l)^H\nabla_{\mathbf{x}} f_j(\mathbf{x}^l,\mathbf{h}^l) \\ &\quad + \tfrac{L_{\mathbf{x}}}{2}\|\mathbf{x}-\mathbf{x}^l\|_2^2 + \tfrac{1}{2}\|\mathbf{x}\|_2^2 + \lambda\|\mathbf{x}\|_1 \\ q_{\mathbf{h}}(\mathbf{h},\mathbf{x}^l,\mathbf{h}^l) &= (\mathbf{h}-\mathbf{h}^l)^H\nabla_{\mathbf{h}} f_j(\mathbf{x}^l,\mathbf{h}^l) \\ &\quad + \tfrac{L_{\mathbf{h}}}{2}\|\mathbf{h}-\mathbf{h}^l\|_2^2 + \tfrac{1}{2}\|\mathbf{h}\|_2^2, \end{aligned} \tag{13}$$

where $\mathbf{x}^l$ and $\mathbf{h}^l$ are lth iterates, and $L_{\mathbf{x}}$ and $L_{\mathbf{h}}$ are step sizes set larger than or equal to the Lipschitz constants of f_j with respect to $\mathbf{x}$ and $\mathbf{h}_j$. We then follow an alternating minimization approach by alternately minimizing $q_{\mathbf{x}}$ and $q_{\mathbf{h}}$, such that,

$$\begin{aligned} \mathbf{x}^{l+1} &= \arg\min_{\mathbf{x}} q_{\mathbf{x}}(\mathbf{x},\mathbf{x}^l,\mathbf{h}^l) \\ &= \tfrac{1}{L_{\mathbf{x}}+1}\mathcal{T}\left(L_{\mathbf{x}}\mathbf{x}^l + \hat{\mathbf{A}}_j^H\mathbf{D}_{\hat{\mathbf{B}}\mathbf{h}^l}^H(\hat{\mathbf{r}}_j - \mathbf{D}_{\hat{\mathbf{B}}\mathbf{h}^l}\hat{\mathbf{A}}_j\mathbf{x}^l);\lambda\right), \end{aligned} \tag{14}$$

$$\begin{aligned} \mathbf{h}^{l+1} &= \arg\min_{\mathbf{h}} q_{\mathbf{h}}(\mathbf{h},\mathbf{x}^{l+1},\mathbf{h}^l) \\ &= \tfrac{1}{L_{\mathbf{h}}+1}\left(L_{\mathbf{h}}\mathbf{h}^l + \hat{\mathbf{B}}^H\mathbf{D}_{\hat{\mathbf{A}}_j\mathbf{x}^{l+1}}(\hat{\mathbf{r}}_j - \mathbf{D}_{\hat{\mathbf{A}}_j\mathbf{x}^{l+1}}\hat{\mathbf{B}}\mathbf{h}^l)\right) \end{aligned} \tag{15}$$

where $\mathcal{T}(\cdot;\lambda)$ is the element-wise soft-thresholding operator with threshold λ.

Note that in radar imaging, the imaging operator matrices $\mathbf{A}_j$ are not random. In fact, every matrix $\mathbf{A}_j$ has a large null space since multiple points in the scene indexed by l can have the same distance $(\|\phi(l)-\phi(n_r)\|_2 + \|\phi(l)-\phi(n_s)\|_2)$ to the transmitter-receiver pair (n_r, n_s). Therefore, for each new measurement we run a relatively small number of stochastic gradient descent iterations in order not to overfit each new data measurement. We summarize our proposed approach in Algorithm 1. Notice that in step 9 of the algorithm, we scale the step size for $\mathbf{x}$ by $\sqrt{j}$ following standard practice in stochastic gradient descent algorithms [11].

IV. Numerical Results

We test the performance of our approach using a simulated target and wall scene as well as using real TWI radar measurements. In both cases, the scene is illuminated using a stepped frequency pulse spanning a 5 GHz bandwidth centered at 3.5 GHz. The antenna array is composed of 36 transmitting and 36 receiving antennas collocated horizontally resulting in one-dimensional multiple input multiple output (MIMO) linear array. The horizontal spacing between the antennas is 4.29 cm giving the array a horizontal aperture of 1.50 meters. The radar scene is divided into a 93×133 grid spanning an area of 2 m

Algorithm 1 Online Blind Deconvolution using Alternating Stochastic Gradient Descent

1: **Input** $\mathbf{r}_j$, $\hat{\mathbf{A}}_j$, $\hat{\mathbf{B}}$, λ, `maxiter`
2: **Output** $\mathbf{x}$, $\mathbf{h}_j$ $\forall j \in \{1,\dots J\}$
3: **Initialize** $j=0$, $\mathbf{h}_0 = [1,0,\dots 0]^T$
4: **repeat**
5: $\quad j = j+1$
6: $\quad \mathbf{x}^0 = \mathbf{x}_{j-1}$
7: $\quad \mathbf{h}^0 = \mathbf{h}_{j-1}$
8: $\quad$ **for** $l=1$ **to** `maxiter` **do**
9: $\quad\quad L_{\mathbf{x}} = \sqrt{j}\|\hat{\mathbf{A}}_j^H\mathbf{D}_{\hat{\mathbf{B}}\mathbf{h}^l}\|_F^2$
10: $\quad\quad \mathbf{x}^{l+1} = \frac{1}{L_{\mathbf{x}}+1}\mathcal{T}\left(L_{\mathbf{x}}\mathbf{x}^l + \hat{\mathbf{A}}_j^H\mathbf{D}_{\hat{\mathbf{B}}\mathbf{h}^l}^H(\hat{\mathbf{r}}_j - \mathbf{D}_{\hat{\mathbf{B}}\mathbf{h}^l}\hat{\mathbf{A}}_j\mathbf{x}^l);\lambda\right)$
11: $\quad\quad L_{\mathbf{h}} = \|\hat{\mathbf{B}}^H\mathbf{D}_{\hat{\mathbf{A}}_j\mathbf{x}^{l+1}}\|_F^2$
12: $\quad\quad \mathbf{h}^{l+1} = \frac{1}{L_{\mathbf{h}}+1}\left(L_{\mathbf{h}}\mathbf{h}^l + \hat{\mathbf{B}}^H\mathbf{D}_{\hat{\mathbf{A}}_j\mathbf{x}^{l+1}}(\hat{\mathbf{r}}_j - \mathbf{D}_{\hat{\mathbf{A}}_j\mathbf{x}^{l+1}}\hat{\mathbf{B}}\mathbf{h}^l)\right)$
13: $\quad$ **end for**
14: $\quad \mathbf{x}_j = \mathbf{x}^l$
15: $\quad \mathbf{h}_j = \mathbf{h}^l$
16: **until** $j \geq J$
17: $\mathbf{x} = \mathbf{x}^J$

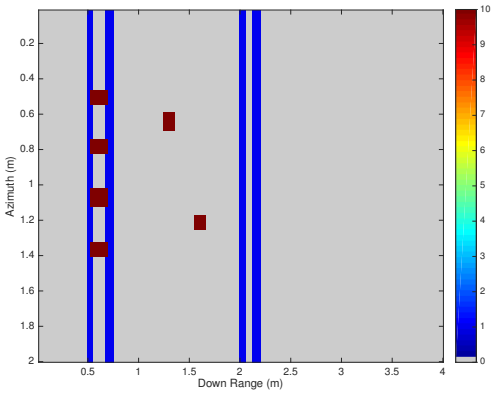

Fig. 1: Simulated scene of a front wall with studs, two targets located behind the wall, and a back wall. The colorbar indicates the reflectivity of the objects in the scene.

azimuth by 4 m down range. The antenna array is centered at location $(0,1)$ and positioned vertically.

A. Simulated scene

We first test our approach using an ideal simulated scene illustrated in Fig. 1. The scene $\mathbf{x}_o$ is composed of two targets located behind a front wall that is supported by four studs as well as a back wall. The colorbar shows the relative reflectivity of the objects in the scene. For each pair of antenna positions (n_r, n_s) indexed by j, we build the imaging operator $\mathbf{A}_j \in \mathbb{C}^{N_t \times M}$ with $N_t = 333$ and $M = N_y N_x = 93 \times 133$. Next, we generate real valued measurement vectors $\mathbf{r}_j = \mathbf{d}_j * \mathbf{A}_j\mathbf{x}_o$, where $\mathbf{d}_j$ is a randomly generated convolution kernel of length $N_h = N_t/10$. We set `maxiter` to 100, and set $\lambda = 50$ when deconvolution is used and $\lambda = 10$ when deconvolution is disabled. The reason for using a smaller λ when deconvolution is disabled was that setting $\lambda = 50$ suppressed also a large portion of the targets in the image. We test two cases, the first in which the convolution kernel $\mathbf{d}_j$ remains constant

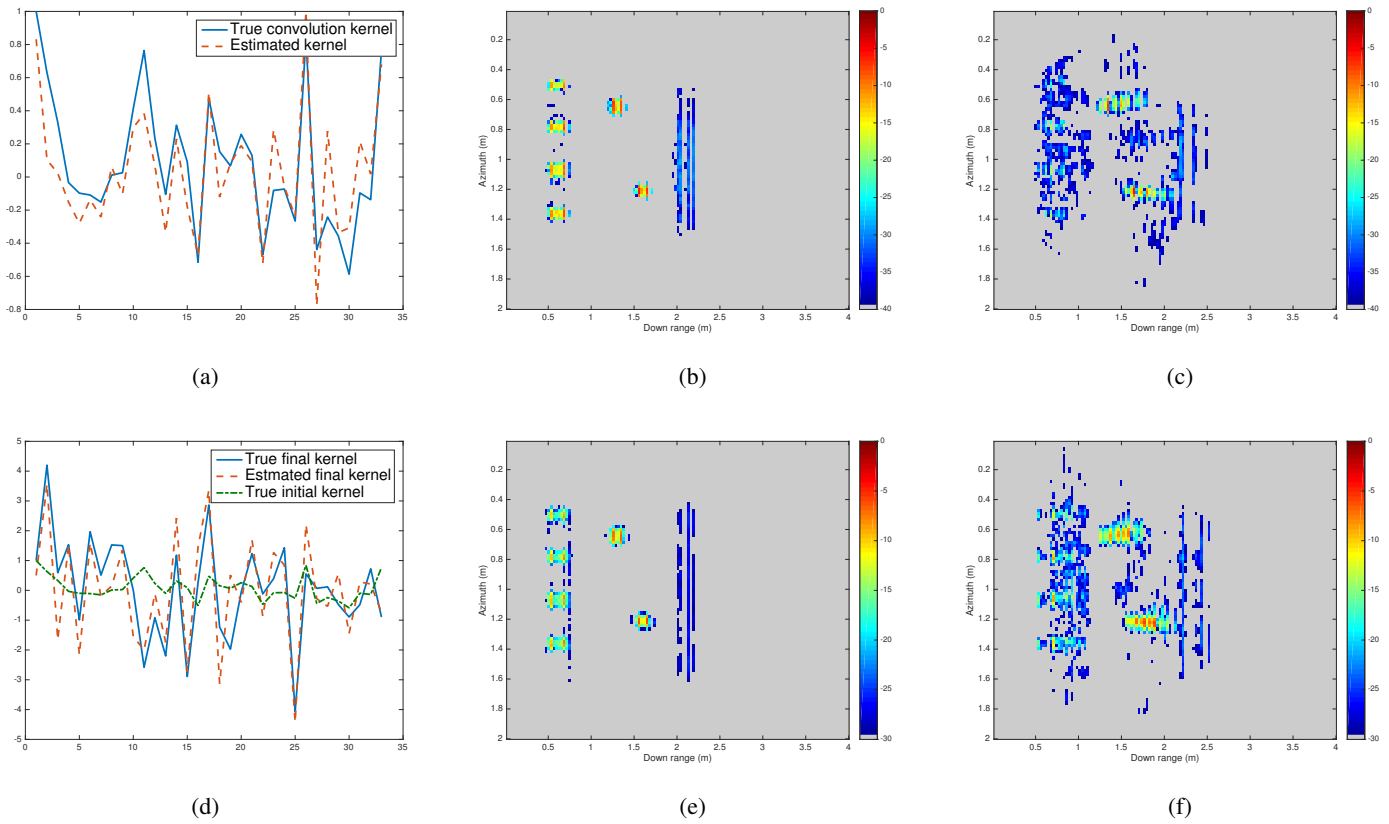

Fig. 2: Blind deconvolution results using the proposed framework applied to the simulated scene when (a)–(c) the convolution kernel is constant, and (d)–(f) the convolution kernel changes smoothly between measurements. The first column shows the true convolution kernel compared to the estimate kernel. The second column shows the reconstructed scene using our alternating stochastic gradient descent approach, and third column shows the reconstruction without performing deconvolution.

for all j, and the second where $\mathbf{d}_j$ changes slowly between measurements.

Fig. 2 illustrates the result of applying the proposed blind deconvolution approach to separate the convolution kernels from the sparse radar image. The figure shows that our method successfully separates the convolution kernels from the image when the kernel is constant and when it changes.

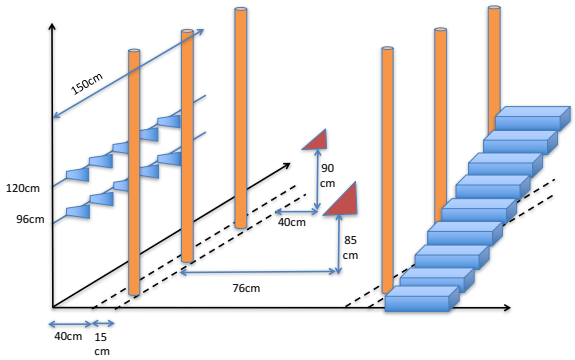

Fig. 3: Schematic of the experimental layout.

B. *Real TWI measurements*

We built a radar setup using two horn antennas mounted on a moving platform. The horn antennas were connected to a signal source, in this case an Agilent 2-Port PNA model 5230A, which measured the scattering parameters of the scene. The PNA was set to sweep over a frequency range from 1–6 GHz and the port output power was set to 5 dBm. Over this range of frequencies the horn antennas have approximately a 40 degree main lobe beam width and a gain near 7 dBi. By moving the antenna positions and repeating the same experiment, we were able to collect radar measurements corresponding to a 36 element virtual one dimensional MIMO array. Additionally, at each position 20 scattering parameter measurements were collected and averaged to reduce the noise floor. The antennas were vertically offset by 24.5 cm so that they can occupied the same horizontal positions. The vertical offset also provided a relatively small aperture in the elevation dimension which allowed us to generate three dimensional radar images. We then used the antenna array to image a real world three dimensional scene similar to the simulated scene described above. Fig. 3 shows a schematic of the scene where two corner reflectors were placed between two walls containing aluminum studs.

The effect of estimating a convolution kernel and removing its impact is evident when we compare the left and right

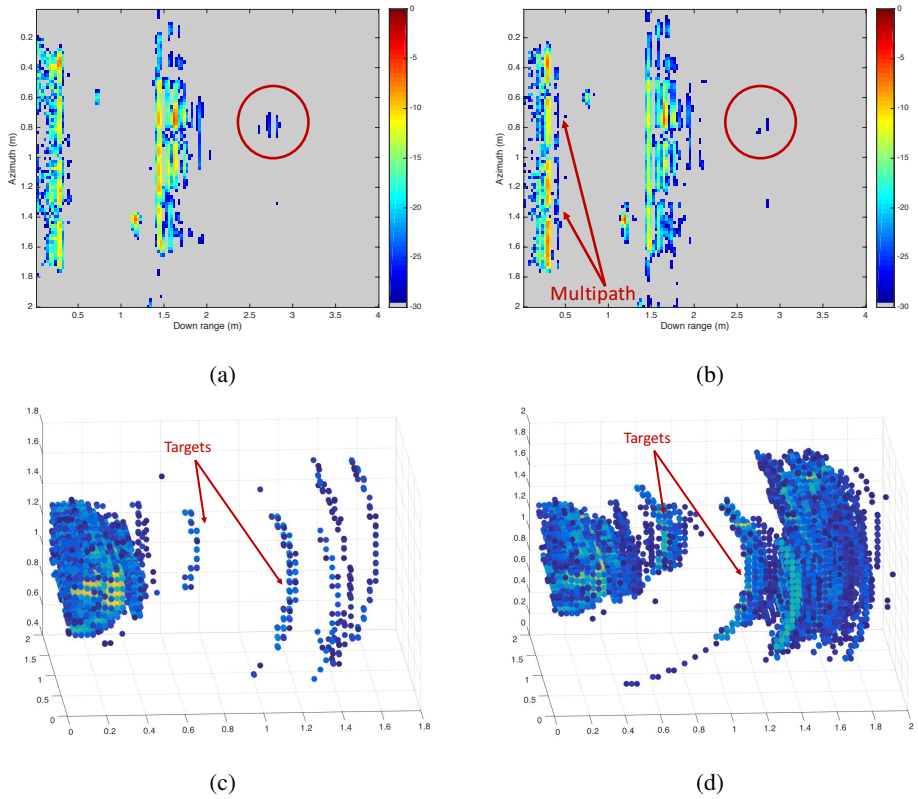

(a) (b) (c) (d)

Fig. 4: (a)–(b) Recovered two dimensional scenes (a) using the proposed approach, and (b) using sequential sparse imaging without deconvolution. (c)–(d) Recovered three dimensional scene (c) using the proposed approach, and (d) using sequential sparse imaging without deconvolution.

columns in Fig. 4. For this dataset, we set `maxiter` to 50 and set $\lambda = 2$. The top row shows the two dimensional imaging results. Notice how the wall multipath is significantly suppressed and internal structures (inside the circle) such as the stair supports appear clearer when deconvolution is employed in Fig. 4(a) compared to Fig. 4(b). The bottom row shows the three dimensional imaging results. The arch-shaped structures appear instead of vertically localized objects due to the small aperture of the antenna array along the vertical axis. In this case, the effect of deconvolution becomes more visible.

V. Conclusion

We presented an alternating stochastic gradient descent algorithm for performing online blind deconvolution in sequential TWI. Our approach extends the recent convex programming formulations for blind deconvolution to the sequential measurement scenario by formulating it as a low-rank tensor recovery problem. Using both simulated and real radar measurements, we demonstrate that our approach effectively removes the front wall ringing effect while maintaining the direct target reflections.

References

[1] P. Setlur, M. Amin, and F. Ahmad, "Multipath model and exploitation in through-the-wall and urban radar sensing," *IEEE Transactions on Geoscience and Remote Sensing*, vol. 49, no. 10, pp. 4021–4034, 2011.

[2] P. C. Chang, *Physics-Based Inverse Processing and Multi-path Exploitation for Through-Wall Radar Imaging*, Ph.D. thesis, Ohio State University, 2011.

[3] P. Setlur, G. Alli, and L. Nuzzo, "Multipath exploitation in through-wall radar imaging via point spread functions," *IEEE Transactions on Image Processing*, vol. 22, 2013.

[4] M. Leigsnering, F. Ahmad, M. Amin, and A. Zoubir, "Multipath exploitation in through-the-wall radar imaging using sparse reconstruction," *IEEE Trans. Aerosp. Electron. Syst.*, vol. 50, no. 2, pp. 920–939, April 2014.

[5] H. Mansour and D. Liu, "Blind multi-path elimination by sparse inversion in through-the-wall-imaging," in *Proc. IEEE 5th Int. Workshop on Computational Advances in Multi-Sensor Adaptive Process. (CAMSAP)*, St. Martin, December 15-18, 2013, pp. 256–259.

[6] M. Leigsnering, F. Ahmad, M. G Amin, and A. M. Zoubir, "CS based specular multipath exploitation in TWRI under wall position uncertainties," in *Proc. 8th IEEE Sensor Array and Multichannel Signal Processing Workshop*, Coruña, Spain, June 22-25, 2014, pp. 481–484.

[7] H. Mansour and U. Kamilov, "Multipath removal by online blind deconvolution in through-the-wall-imaging," in *IEEE International Conference on Acoustics, Speech, and Signal Processing (ICASSP)*, March 2016.

[8] A. Ahmed, B. Recht, and J. Romberg, "Blind deconvolution using convex programming," *IEEE Transactions on Information Theory*, vol. 60, no. 3, pp. 1711–1732, March 2014.

[9] S. Ling and T. Strohmer, "Self-calibration and biconvex compressive sensing," *Inverse Problems*, vol. 31, no. 11, pp. 115002, 2015.

[10] Srebro N., *Learning with matrix factorizations*, Ph.D. thesis, Cambridge, MA, USA, 2004, AAI0807530.

[11] H. J. Kushner and G. Yin, *Stochastic approximation and recursive algorithms and applications*, Applications of mathematics. Springer, New York, 2003.